State-to-state rotational relaxation rate constants for CO+Ne from IR–IR double-resonance experiments: Comparing theory to experiment

David A. Hostutler,[a] Tony C. Smith, and Gordon D. Hager
*Air Force Research Laboratory/Directed Energy Directorate, Kirtland Air Force Base,
New Mexico 87117-5776*

George C. McBane
Department of Chemistry, Grand Valley State University, Allendale, Michigan 49401

Michael C. Heaven
Department of Chemistry, Emory University, Atlanta, Georgia 30322

IR–IR double-resonance experiments were used to study the state-to-state rotational relaxation of CO with Ne as a collision partner. Rotational levels in the range $J_i = 2-9$ were excited and collisional energy transfer of population to the levels $J_f = 2-8$ was monitored. The resulting data set was analyzed by fitting to numerical solutions of the master equation. State-to-state rate constant matrices were generated using fitting law functions. Fitting laws based on the modified exponential gap (MEG) and statistical power exponential gap (SPEG) models were used; the MEG model performed better than the SPEG model. A rate constant matrix was also generated from scattering calculations that employed the *ab initio* potential energy surface of McBane and Cybulski [J. Chem. Phys. **110**, 11 734 (1999)]. This theoretical rate constant matrix yielded kinetic simulations that agreed with the data nearly as well as the fitted MEG model and was unique in its ability to reproduce both the rotational energy transfer and pressure broadening data for Ne–CO. The theoretical rate coefficients varied more slowly with the energy gap than coefficients from either of the fitting laws. © *2004 American Institute of Physics.* [DOI: 10.1063/1.1687314]

I. INTRODUCTION

The CO–Ne complex has received considerable attention in the last several years. Winnewisser *et al.*[1] and Walker *et al.*[2] have reported pure rotational spectra of the van der Waals complex. The IR spectrum of this species has been observed by McKellar and co-workers.[3,4] In addition to spectroscopic studies, CO+Ne has been the subject of several collisional dynamic studies. Pressure broadening,[5,6] virial,[7,8] transport,[9–11] and state-to-state cross section data[12,13] are available in the literature.

Several CO–Ne potential energy surfaces (PESs) have also been presented.[14–16] The CO–Ne complex is a good candidate for *ab initio* studies. The three heavy atoms are small enough that very-high-level electronic calculations using large basis sets are not prohibitively time consuming. In 1997, Moszynski *et al.*[14] presented a PES of CO–Ne using symmetry-adapted perturbation theory (SAPT). The group concluded that the complex was near T shaped with a minimum near -54 cm^{-1}. Two more surfaces derived using the supermolecule method were published in 1999. The first, by McBane and Cybulski,[15] used a large basis set at the CCSD(T) level of theory. It did not describe the ground-state structure of Ne–CO as well as the SAPT potential, but comparisons to the scattering data indicated that it described the repulsive part of the interaction better than SAPT. The second surface, reported that year by Subramanian *et al.*,[16] used

a smaller basis set than McBane and Cybulski and the MP4 level of theory. This group did not report an analytical fit and did not comment on the agreement with experimental results.

Our group is currently measuring state-to-state rotational relaxation rate constants for CO with various collision partners using IR–IR double-resonance experiments. This is the third project in a series; results for CO+CO (Ref. 17) and CO+He (Ref. 18) have already been presented. This paper describes our CO+Ne double-resonance data and modeling. After the data were collected, the full rotational relaxation rate constant matrix was approximated by computer simulations of our data using the master equation and two common fitting laws: the modified exponential gap (MEG) and the statistical power exponential gap (SPEG) models. Additionally, purely theoretical rate constants determined from the CCSD(T) potential energy surface of McBane and Cybulski[15] were compared to both our kinetics data and to CO+Ne pressure broadening data.

II. EXPERIMENT

Because it is sensitive to individual rate constants, the pump–probe double-resonance technique[19] is useful for monitoring rotational energy transfer (RET). Our experiment was carried out in a 296-K gas cell containing 0.25 torr of CO (Air Products, UHP) and 0.50 torr of Ne (Spectra Gases, UHP). During the experiment, a pump laser pulse, which was resonant with a selected transition of the first overtone band (2–0), prepared a population of molecules in a single

---

[a]Author to whom correspondence should be addressed.

7483

TABLE I. Coefficients for Eq. (1), which represents the time-dependent population profiles.

J_i	J_f	a^a	b^b	c^b	d^b	J_i	J_f	a	b	c	d
2	3	40.7087	0.003157	0.008915	0.001454	6	2	7.9313	0.004321	0.001974	0.002349
2	4	33.6912	0.003180	0.006295	0.001599	6	3	25.7596	0.002253	0.005853	0.001667
2	5	41.6091	0.002370	0.007003	0.001568	6	4	19.1714	0.004083	0.004599	0.002542
2	6	14.8988	0.004422	0.002035	0.002401	6	5	10.9019	0.009707	0.000776	0.001797
2	7	39.0913	0.001661	0.005145	0.001362	6	7	11.6403	0.008241	0.000966	0.002291
2	8	11.9187	0.003473	0.001189	0.002443	6	8	10.0222	0.008170	0.000874	0.003496
3	2	24.0438	0.003633	0.007645	0.001669	7	2	7.4221	0.005823	0.002442	0.003382
3	4	35.1349	0.003197	0.007151	0.001724	7	3	8.6747	0.004714	0.001062	0.002047
3	5	42.3232	0.002716	0.007693	0.001687	7	4	9.0656	0.007182	0.000715	0.002180
3	6	35.3386	0.002443	0.006249	0.001847	7	5	10.1692	0.008640	0.000646	0.001927
3	7	20.4064	0.002772	0.002972	0.001991	7	6	10.5340	0.009746	0.000765	0.002499
3	8	11.6978	0.003717	0.001196	0.002606	7	8	11.0607	0.009091	0.001176	0.003099
4	2	24.0690	0.003272	0.007803	0.001701	8	2	6.4718	0.004599	0.001551	0.003091
4	3	33.9443	0.003113	0.008081	0.001634	8	3	14.6834	0.002628	0.003403	0.002166
4	5	45.4953	0.002903	0.008267	0.001661	8	4	16.8941	0.002728	0.003238	0.002195
4	6	34.8549	0.002880	0.005981	0.001800	8	5	9.0525	0.007559	0.000364	0.001930
4	7	40.5052	0.001957	0.006537	0.001655	8	6	12.4743	0.006527	0.002310	0.004223
4	8	12.6836	0.004011	0.001476	0.002537	8	7	11.1232	0.009401	0.001020	0.002845
5	2	16.5485	0.003222	0.005627	0.001981	9	2	5.5131	0.004922	0.001090	0.003905
5	3	30.1540	0.002625	0.007466	0.001744	9	3	7.9630	0.003594	0.001021	0.002592
5	4	34.7144	0.002831	0.007562	0.001850	9	4	9.1640	0.004259	0.001087	0.003175
5	6	36.9941	0.002923	0.007334	0.002044	9	5	11.5296	0.003863	0.001384	0.002691
5	7	31.6740	0.002841	0.006345	0.002212	9	6	26.7508	0.002409	0.005157	0.002225
5	8	24.7787	0.002651	0.004796	0.002293	9	7	12.9511	0.006608	0.002622	0.004506
						9	8	11.0695	0.009529	0.001029	0.002704

[a]Parameter has units of number density (molecules cm^{-3}). Sufficient digits are quoted to reproduce data to full accuracy.
[b]Parameters have units of ns^{-1}.

rovibrational level of CO ($\nu=2$). Since the vibrational frequency of carbon monoxide is large, the initial thermal population in $\nu=2$ is negligible so that clean population of a single vibration–rotation level could be achieved. A continuous-wave (cw) probe laser was tuned to various transitions of the (3–2) absorption band. As RET processes redistributed the population within the CO ($\nu=2$) rotational manifold, the time-dependent transmittance of the probe laser was recorded as our double-resonance signal. Details of the IR–IR pump–probe apparatus and procedure have been described elsewhere[17,18] and will not be repeated here.

III. RESULTS

A. Data reduction

The raw pump–probe data are influenced by more than just the rotational relaxation. The two other factors that contribute to the observed transient absorption signals are vibrational relaxation and velocity relaxation. Our earlier papers[17,18] describe the approach we use to remove those effects from the transient absorption signals, converting each trace into a "population profile" $P(J_i,J_f,t)$ that is proportional to the time-varying population in level J_f that would be observed after excitation of level J_i if no vibrational relaxation was taking place. The population profiles are normalized so that the long-time asymptote of each corresponds to the population in J_f at 296 K rotational equilibrium.

Data were collected for 49 different J_i,J_f pairs, with $2 \leq J_i \leq 9$ and $2 \leq J_f \leq 8$. To make the data more manageable each population profile was fit to the expression

$$\bar{P}(J_i,J_f,t)=a\left[1-\exp(-bt)-\frac{c}{c+d}\left(1 + \frac{b\exp[-(c+d)t]-\exp(-bt)(c+d)}{c+d-b}\right)\right], \quad (1)$$

where a, b, c, and d are adjustable parameters. The values for the fitted parameters for each of the profiles are given in Table I.

B. Simulation of rotational relaxation kinetics with empirical RET models

Rotational relaxation in $\nu=2$ was simulated using a system of coupled differential equations (the master equation) of the form

$$\frac{dN_J}{dt}=\sum_{J'} (k_{J\leftarrow J'}^{CO-CO}N_{J'}-k_{J'\leftarrow J}^{CO-CO}N_J)[CO]$$
$$+\sum_{J'} (k_{J\leftarrow J'}^{CO-Ne}N_{J'}-k_{J'\leftarrow J}^{CO-Ne}N_J)[Ne], \quad (2)$$

where N_J is the population in the J level and $k_{J\leftarrow J'}^{CO-CO}$ and $k_{J\leftarrow J'}^{CO-Ne}$ are the CO+CO and CO+Ne rotational relaxation rate constants, respectively. Values for the CO+CO rate constants ($k_{J\leftarrow J'}^{CO-CO}$) were taken from the previous work of Phipps *et al.*[17]

The master equation properly incorporates all rotational levels. However, only those rotational levels that contain significant thermal populations need to be included to provide an accurate description of rotational relaxation. Since $\sim$97%

TABLE II. Experimentally determined parameters for the MEG and SPEG fitting laws and the variance between computer simulations and our experimental data.

| Parameters | Fitting results[a] | | Theoretical results |
	MEG	SPEG	CCSD(T)
α (10^{-11} cm^3 molecule^{-1} s^{-1})	4.51(48)	18.1(3.0)	....
β	1.73(19)	0.77(15)	....
δ	1.08(16)	0.502(40)	....
SSD[b]	0.152	0.267	0.172

[a]Experimental values from this work. Values in parentheses are estimated errors, which were obtained by varying the parameter until a 10% increase in the SSD was obtained while holding all other parameters constant.
[b]Sum of squared deviations between experimental and computer simulated population profiles.

of the rotational population resides in rotational levels below $J < 20$ at 297 K, we restricted the model to consider $J \leq 29$. A matrix of 900 rate constants was then needed to specify the system of equations. Applying detailed balance and setting the diagonal elastic rates to zero reduces the problem to that of finding 435 independent rate constants, but this is still too many parameters to be determined from the data collected in these experiments. Therefore, we have applied the usual method of representing the CO+Ne rotational–translation relaxation rate constant matrix with fitting law functions.

The full CO+Ne rotational relaxation rate constant matrix was extracted using two common fitting laws: the modified exponential gap[20–22] and statistical power exponential gap[21–23] models. Our previous CO+CO RET paper gives a detailed description of our technique and procedure for using these fitting laws.[17] For upward transitions ($j > i$), the MEG law had the form

$$k_{J \leftarrow i} = \alpha \exp\left(\frac{-\beta \Delta E_{ji}}{kT}\right) \left(\frac{1 + \dfrac{2E_i}{\gamma kT}}{1 + \dfrac{2E_i}{kT}}\right)^2 \qquad (3)$$

and the SPEG law was expressed as

$$k_{j \leftarrow i} = \alpha \exp\left(\frac{-\beta \Delta E_{ji}}{kT}\right) \left(\frac{\Delta E_{ji}}{B_{\nu=2}}\right)^{-\gamma}, \qquad (4)$$

where α, β, and γ are the adjustable parameters in each case. The rate coefficients for downward transitions ($j < i$) were obtained by detailed balance.

The master equation was solved numerically using the fourth-order Runge–Kutta method, and the MEG and SPEG fitting law expressions were fitted to the $\bar{P}(J_i, J_f, t)$ curves. A computer program was written that independently varied the adjustable fitting parameters for each of the fitting laws to minimize the sum of the squared deviations (SSD). The program terminated when the SSD between the master equation solutions and the $\bar{P}(J_i, J_f, t)$ curves, sampled at 100 points between 0 and 4 μs, reached a minimum.

The resulting values for the best-fit parameters from computer simulations of our CO+Ne data set, using the MEG and SPEG models, are given in Table II. The MEG computer simulations reproduced the experimentally deter-
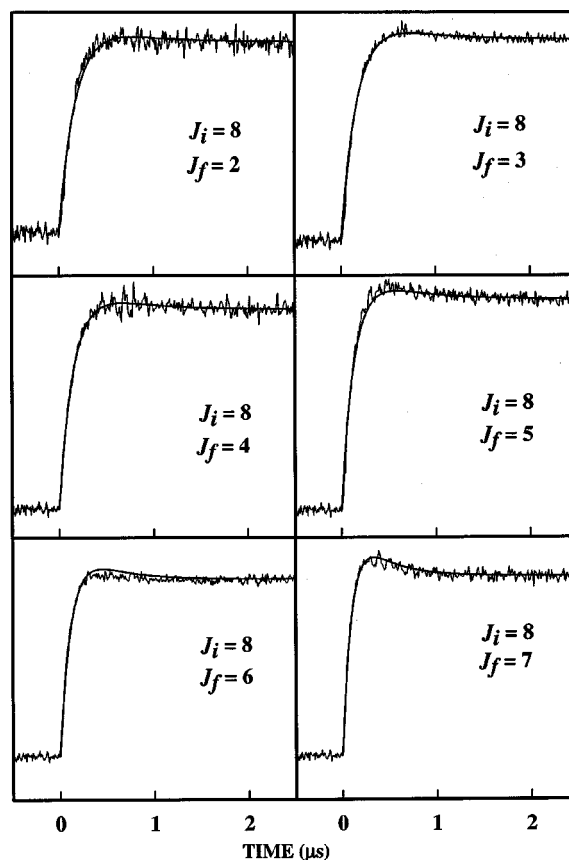

FIG. 1. Time-dependent rotational populations for $J_f = 2-7$ following excitation of $J_i = 8$. The smooth lines through the data are from computer simulations that used rate constants represented by the MEG fitting law model.

mined $P(J_i, J_f, t)$ data better than the SPEG model, with a 43% decrease in the SSD between the computer simulations and the reduced experimental data. Figure 1 shows simulations using the MEG model (solid line) for a series of population profiles with $J_i = 8$ and $2 \leq J_f \leq 7$. The asymptotic values of the data and the fitted curves in Fig. 1 are equal to the equilibrium populations. The information in the comparison is therefore in the initial slope of the fitted profile and the shape of its approach to equilibrium. The simulations using the MEG model reproduce our CO+Ne kinetics data very well with most of the simulation traces within the experimental noise.

C. *Ab initio* rate coefficients

We also calculated the matrix of RET rate coefficients directly from an *ab initio* model of the Ne–CO potential energy surface. Since the experiment was carried out with CO in $\nu = 2$, it would be best to use a potential surface averaged over the $\nu = 2$ vibrational motion of CO. However, none of the existing Ne–CO potential surface models includes the CO vibrational coordinate. In comparison to the results from scattering studies,[12,13] the CCSD(T) surface of McBane and Cybulski appeared to give a better description of the repulsive wall, so we selected it for simulation of the double-resonance data.

Time-independent coupled-channel scattering calculations were carried out with the MOLSCAT program of Hutson

and Green.[24] The "S2" potential surface of McBane and Cybulski was used to describe the intermolecular potential. That surface treats CO as a rigid rotor with a C–O internuclear distance equal to the diatomic potential minimum. The asymptotic rotational energy levels used in the calculation were those of free CO in $\nu=2$. The $\nu=2$ rotational constants were obtained from the work of Maki, Wells, and Jennings.[25] The two-dimensional potential was expanded using 16 Legendre polynomial terms with radially dependent expansion coefficients.

The close-coupled equations were solved using the hybrid log-derivative Airy propagator of Alexander and Manolopolous.[26] Close-coupled (CC) calculations were performed for all total energies below the $J=21$ threshold (870 cm^{-1}) and, in a few instances, for energies up to 1500 cm^{-1}. The rotational basis sets included all open channels and at least two closed channels. Most calculations at energies above 870 cm^{-1} used the coupled-states (CS) approximation of McGuire and Kouri,[27] and the basis sets then included at least one closed channel. All propagations were carried out to a center-of-mass separation of at least 28 Å, though many calculations were extended to larger distances to ensure that the asymptotic boundary conditions were imposed beyond the centrifugal barrier. The partial-wave sum was terminated when the elastic cross sections had converged to at least 1 Å^2 and the inelastic cross sections to 0.01 Å^2. At the highest energies in our calculations (2182 cm^{-1}), the maximum total angular momentum included in the partial-wave sum was $179\hbar$.

The grid of energies used in the calculations was selected to capture most of the variations in cross sections just above the energy thresholds for channel openings for the purpose of thermal averaging. Just above each threshold, beginning with $J=1$, a series of total energies was used whose spacings began at 1 cm^{-1} and increased to larger values as the cross sections became smoother. Each series was terminated when the next threshold was reached.

Calculations were only performed for the dominant ^{20}Ne isotope. Test calculations at a few energies indicated that inclusion of the minor ^{22}Ne isotope would modify the calculated rate coefficients by less than 1%.

D. Thermal averaging

Thermally averaged cross sections were evaluated according to the expression

$$\sigma_{if}(T) = (kT)^{-2} \int_0^\infty \varepsilon_t \sigma_{if}(\varepsilon_t) \exp(-\varepsilon_t/kT) d\varepsilon_t, \qquad (5)$$

where ε_t is the precollision center-of-mass translational energy. The integration was carried out using the trapezoidal rule, and the cross section was assumed to be zero for all translational energies above the highest in our computed set. The truncation of the integral introduces negligible error for rate coefficients involving only $J<21$. For higher rotational levels, truncation causes a systematic underestimation of the rate coefficients. The thermalized cross sections were multiplied by the average collision speed $\langle v \rangle = (8kT/\pi\mu)^{1/2}$ to convert them to state-to-state rate coefficients.
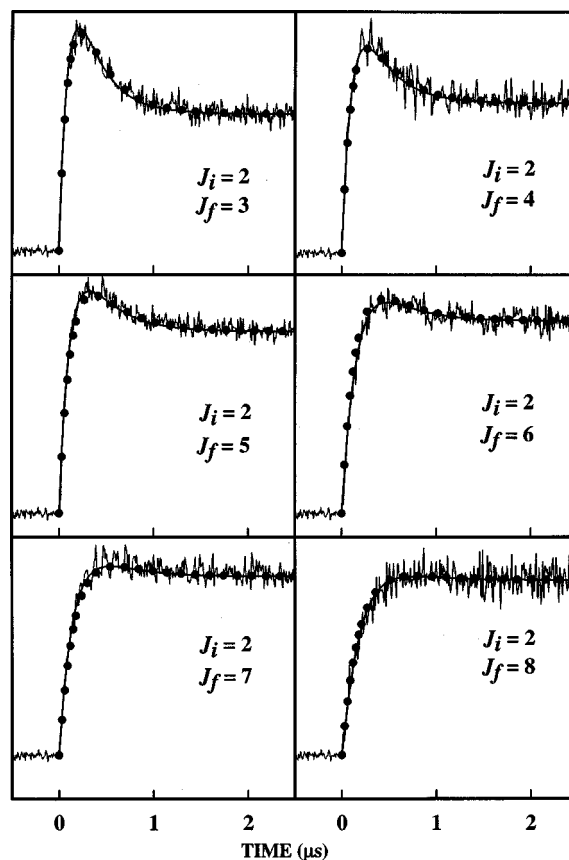

FIG. 2. Time-dependent rotational populations for $J_f=3-8$ following excitation of $J_i=2$. The figure also includes computer simulations of the CO + Ne data using rate constants derived from the CCSD(T) potential energy surface (Ref. 15) (solid lines) and rate constants represented by the MEG fitting law model (solid points).

The CCSD(T) *ab initio* rate constants were inserted into the master equation, which was then solved to simulate the population evolutions. Figure 2 shows a comparison of the experimental curves and computer simulations using the rate matrices generated from the CCSD(T) potential energy surface and the MEG model. In the figure the CCSD(T) predicted populations are represented by the smooth curves through the $\bar{P}(J_i,J_f,t)$ data while the MEG simulations are represented by solid points. The agreement between the CCSD(T) theoretical rate constant matrix model and the experimental data was very favorable, with a SSD of 0.172, as listed in Table II.

IV. DISCUSSION

Graphical representations of the CO+Ne rate constant matrices from the MEG, SPEG, and CCSD(T) models are shown in Figs. 3(a), 3(b), and 3(c). The CCSD(T) and MEG rate constant displays are very similar in shape. Computer simulations using these rate constant matrices were found to reproduce the experimental data much more accurately than the SPEG model. The most distinctive feature of the CCSD(T) and MEG rate matrices is that the rate constants near the diagonal have a weak dependence on the energy gap. The rate constant matrix generated from the SPEG fit-
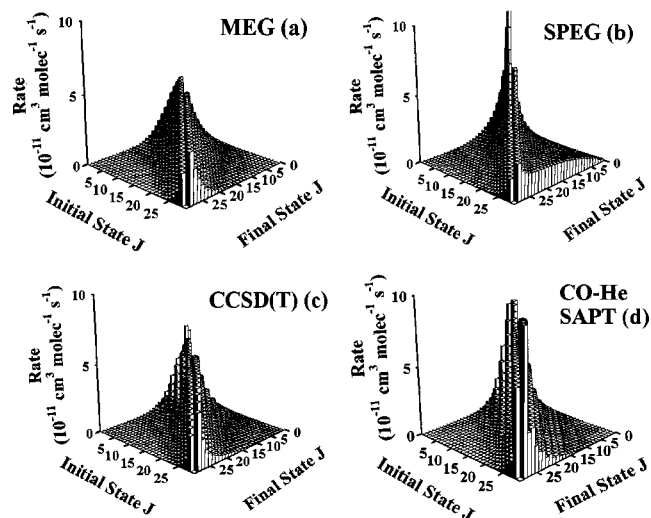
FIG. 3. Bar graph representations of rate constant matrices generated from the MEG, SPEG, and CCSD(T) models are displayed in plots *a*, *b*, and *c*, respectively. Rate constants predicted from the CO–He SAPT potential energy surface (Ref. 33) are displayed in plot *d*.
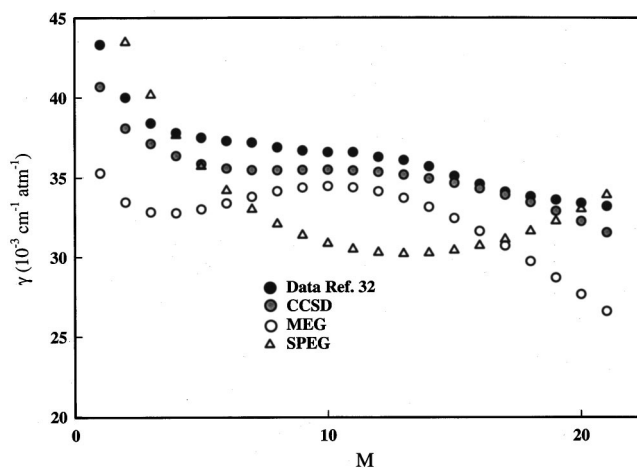

FIG. 4. Simulations of the CO+Ne pressure broadening data using the predictions for the CCSD(T) potential energy surface, and the MEG and SPEG fitting law models. Positive values of *M* indicate *R*-branch lines with $J=M-1$. The experimental CO–Ne pressure broadening data were taken from Ref. 32 and are illustrated by the solid black circles. The predictions from the CCSD(T) PES are represented by gray solid circles, and the MEG and SPEG fitting laws are represented by open circles and triangles, respectively.

ting law function is much more dependent on the energy gap and overestimates the low *J* rate coefficients while underestimating higher *J* coefficients.

As in our previous work on CO+He RET, we find that the time-resolved kinetic data do not define a unique matrix of state-to-state transfer rate constants. Consequently, we have used the three different rate constant sets to simulate the pressure broadening coefficients for CO+Ne. This provides an independent test of each model. Following the work of previous investigators, we calculated the pressure broadening coefficients using the assumptions that the major contributor to pressure broadening for CO was rotationally inelastic collisions [the diagonal rate constants ($k_{J \leftarrow J}^{CO-Ne}$) were set to zero] and that the RET rate constants were vibrationally independent.[28,29] The pressure broadening coefficients are then given by[29]

$$\gamma(J',J'') = \frac{1}{4\pi}\left(\sum_{J'_f} k_{J'_f \leftarrow J'} + \sum_{J''_f} k_{J''_f \leftarrow J''} \right), \quad (6)$$

where J' and J'' are the upper and lower *J* values for a specific rovibrational line.

The insensitivity of CO line broadening coefficients to the vibrational transition is well established.[30] To check that the elastic contributions to the line broadening are negligible, we carried out a limited set of additional scattering calculations on the CCSD(T) potential surface and used them to calculate pressure broadening coefficients with both Eq. (6) and the accurate Shafer–Gordon theory[31] as implemented in MOLSCAT. Calculations were performed for the pure rotational 5←4 and 18←19 transitions in the ground vibrational state of CO, using coupled-states calculations and a 50-cm^{-1} translational energy grid. Pressure broadening coefficients calculated by the two methods from this single set of scattering calculations differed by less than 2%.

Pressure broadening coefficients calculated with Eq. (6) from the CCSD(T), MEG, and SPEG rate constant matrices are compared with the experimental data of Bouanich[32] in

Fig. 4. The CCSD(T) *ab initio* rate constant matrix (solid gray circles) reproduced the experimental data (black solid circles) much better than the rate matrices generated from the MEG or SPEG fitting laws. The experimental data and the CCSD(T) predicted pressure broadening linewidths both have only a weak *J* dependence. The pressure broadening coefficients generated from the MEG rate matrix are slightly more *J* dependent than those produced from the CCSD(T) potential energy surface and the values are too small. The pressure broadening coefficients generated from the SPEG fitting law rate matrix compare poorly to the experimental data. This model overestimates the coefficients for low values of *J* and underestimates them in the intermediate-*J* range. The CCSD(T) rate matrix compares most favorably with both the kinetics and pressure broadening data.

The complete CCSD(T) rate constant matrix for values of $J \leqslant 20$ is listed in Table III. Note that the rate constants for removal of population from a given level are about 2.5×10^{-11} cm^3 s^{-1}. This value is similar to the rate constant for hard-sphere collisions, indicating that RET occurs on almost every collision. This observation provides more support for the approximation of neglecting the elastic CO+Ne collisions in calculating the pressure broadening coefficients.

Figure 4 shows that the total rate constants for transfer out of the initial levels $J_i = 2-9$ for the MEG model are smaller than the corresponding rate constants derived from the CCSD(T) calculations. Given that the two models provide comparable simulations of the kinetic data, this was somewhat surprising. The rate at which the population profiles rise at short pump–probe delay times should provide a direct reflection of the rate of transfer out of the initially populated level. Hence it would be expected that the rise times of the curves using the MEG and CCSD(T) models would be perceptibly different. This is true of the simulations, but the noise on the steep rising edges of the experi-

TABLE III. Theoretical CO–Ne inelastic rotational relaxation rate constants calculated from the CCSD(T) PES. Rate constants in units of 10^{-11} cm^3 molecule^{-1} s^{-1}.

$J_i\backslash J_f$	0	1	2	3	4	5	6	7	8	9	10	11	12	13	14	15	16	17	18	19	20
0	0.00	1.98	1.33	0.68	0.34	0.46	0.17	0.28	0.13	0.16	0.11	0.10	0.09	0.06	0.06	0.05	0.04	0.03	0.03	0.02	0.02
1	5.83	0.00	3.26	2.26	1.66	0.73	1.11	0.45	0.65	0.37	0.37	0.29	0.23	0.22	0.16	0.15	0.12	0.10	0.09	0.07	0.06
2	6.27	5.24	0.00	3.79	2.63	2.29	0.99	1.47	0.68	0.85	0.55	0.50	0.42	0.32	0.31	0.23	0.21	0.17	0.14	0.12	0.10
3	4.29	4.82	5.03	0.00	4.06	2.80	2.62	1.19	1.64	0.85	0.95	0.67	0.57	0.51	0.37	0.36	0.27	0.24	0.20	0.16	0.14
4	2.53	4.23	4.16	4.86	0.00	4.20	2.88	2.77	1.33	1.69	0.97	0.99	0.75	0.60	0.56	0.41	0.38	0.30	0.25	0.22	0.18
5	3.83	2.07	4.04	3.73	4.68	0.00	4.29	2.88	2.81	1.42	1.69	1.03	0.99	0.79	0.61	0.57	0.43	0.38	0.31	0.26	0.22
6	1.51	3.33	1.85	3.70	3.40	4.54	0.00	4.40	2.82	2.81	1.46	1.66	1.07	0.97	0.81	0.61	0.56	0.43	0.37	0.31	0.26
7	2.53	1.36	2.79	1.71	3.32	3.09	4.47	0.00	4.54	2.74	2.78	1.47	1.59	1.08	0.92	0.80	0.59	0.54	0.43	0.36	0.31
8	1.17	1.95	1.25	2.29	1.56	2.96	2.80	4.44	0.00	4.70	2.65	2.73	1.47	1.51	1.09	0.87	0.78	0.58	0.52	0.42	0.35
9	1.34	1.04	1.50	1.13	1.88	1.41	2.65	2.54	4.45	0.00	4.85	2.56	2.66	1.46	1.42	1.08	0.82	0.75	0.57	0.49	0.41
10	0.85	0.97	0.89	1.16	0.99	1.55	1.26	2.37	2.31	4.47	0.00	5.00	2.48	2.57	1.47	1.33	1.07	0.79	0.71	0.55	0.47
11	0.65	0.69	0.72	0.74	0.91	0.85	1.28	1.12	2.13	2.11	4.48	0.00	5.14	2.42	2.47	1.47	1.24	1.04	0.76	0.67	0.53
12	0.51	0.47	0.54	0.54	0.60	0.71	0.72	1.06	1.00	1.91	1.94	4.49	0.00	5.27	2.38	2.36	1.48	1.17	1.00	0.74	0.64
13	0.32	0.38	0.34	0.41	0.41	0.48	0.56	0.61	0.88	0.90	1.71	1.80	4.49	0.00	5.39	2.36	2.25	1.48	1.12	0.96	0.72
14	0.26	0.23	0.28	0.25	0.31	0.31	0.39	0.43	0.52	0.72	0.81	1.52	1.68	4.48	0.00	5.50	2.37	2.14	1.47	1.08	0.92
15	0.15	0.18	0.16	0.20	0.19	0.23	0.24	0.31	0.34	0.45	0.60	0.74	1.36	1.59	4.46	0.00	5.58	2.40	2.04	1.45	1.05
16	0.11	0.11	0.12	0.12	0.14	0.14	0.17	0.18	0.24	0.27	0.38	0.49	0.67	1.20	1.53	4.43	0.00	5.64	2.44	1.96	1.42
17	0.07	0.07	0.08	0.08	0.09	0.10	0.10	0.13	0.14	0.19	0.22	0.32	0.42	0.62	1.07	1.48	4.38	0.00	5.65	2.48	1.89
18	0.05	0.05	0.05	0.05	0.05	0.06	0.07	0.08	0.09	0.11	0.15	0.18	0.27	0.35	0.56	0.96	1.44	4.30	0.00	5.65	2.51
19	0.03	0.03	0.03	0.03	0.03	0.04	0.04	0.05	0.06	0.07	0.09	0.12	0.15	0.23	0.31	0.51	0.86	1.41	4.20	0.00	5.59
20	0.02	0.02	0.02	0.02	0.02	0.02	0.03	0.03	0.03	0.04	0.05	0.07	0.09	0.12	0.19	0.27	0.46	0.78	1.36	4.08	0.00

mental data precluded an accurate definition of the initial slopes. Improved data could not be obtained by simply changing the gas composition. If the pressure of Ne was reduced, the kinetics were dominated by CO+CO collisions. Conversely, attempts to mitigate this problem by reducing the CO pressure degraded the signal-to-noise ratio. Hence the error range for the total removal rate constants derived from the kinetic data alone was on the order of 20%.

In our recent study of CO+He rotational relaxation[18] using pump–probe double resonance, we generated the CO+He rate constant matrix from the symmetry-adapted perturbation theory (SAPT) potential energy surface of Heijmen *et al.*[33] The SAPT rate constant matrix reproduced both the CO+He kinetics and pressure broadening data very well. The CO+He room-temperature pressure broadening data is almost J independent, revealing only a weak dependence on the energy gap.[18] As indicated by the rate constants along the diagonal of each matrix, the CCSD(T) rate constant matrix for CO+Ne [shown in Fig. 3(c)] is slightly more dependent on the energy gaps than the CO+He SAPT rate matrix [Fig. 3(d)]. It appears that a weak dependence of the energy transfer rate constants on the energy gaps is a characteristic of impulsive collisions where the dominant interaction between the collision pair occurs at short range on the repulsive wall of the intermolecular potential. The slightly greater dependence of the CO+Ne rate constants on the energy gaps, as compared to CO+He, is consistent with the fact that the slower CO+Ne collisions are not as impulsive and the long-range attraction between the collision pair is greater. The inelastic cross sections for Ne+CO collisions are larger than the corresponding He cross sections; for example, the $3\rightarrow8$ cross section at 210.55 cm^{-1} is 1.39 Å^2 for He and 3.35 Å^2 for Ne. However, the larger cross sections are compensated by the higher He–CO collision rate, so that the room-

temperature CO+Ne rotational relaxation rate constants are slightly slower than those of CO+He.

The rate coefficients for transitions with small to moderate values of $|\Delta J|$ generated from the CO+Ne CCSD(T) *ab initio* potential show a small preference for transitions with odd values of ΔJ. This trend is illustrated in Fig. 5 where the rate constants for transfer from $J_i=5$ and 10 are plotted as a function of J_f. The propensity for odd ΔJ transitions survives the thermal averaging because it holds for a broad range of collision energies. A propensity for odd ΔJ transitions was also observed in the CO+He rate constant matrix,
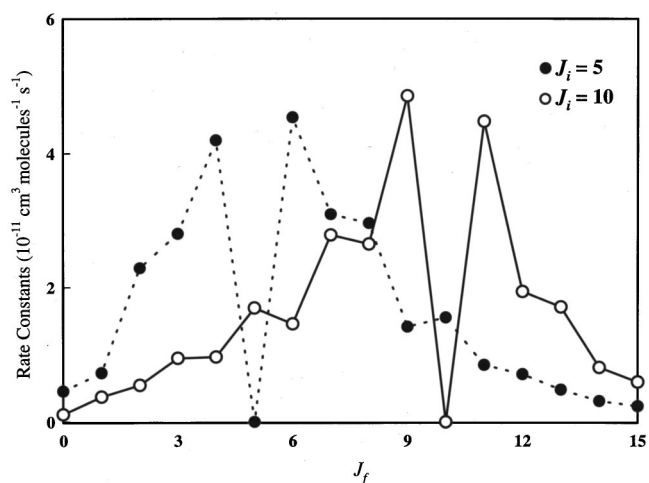

FIG. 5. Rate constants derived from the CCSD(T) potential energy surface. The solid points and open circles correspond to $J_i=5$ and 10, respectively. The maximum in the Boltzmann distribution occurs at $J=7$. Hence the rate constants for $J_i=5$ favor upward transfer while those for $J_i=10$ favor downward transfer. The rate constants show a weak preference for odd-ΔJ transitions.

generated from the SAPT potential energy surface, but there the degree of modulation was more pronounced. Conversely, the data for CO+CO RET collisions exhibit a preference for even ΔJ transitions. These symmetry propensies reflect the symmetry properties of the intermolecular potentials over the range of intermolecular separations that are most important for the energy-transfer processes. Hence the even ΔJ preference of CO+CO reflects the symmetry of the interaction over both the repulsive and attractive parts of the surface, since they both contribute importantly to the rotational energy transfer. CO+He and CO+Ne rotational relaxations are both dominated by dynamics on the repulsive wall, and the shape of that wall produces odd ΔJ propensies in both cases. Unfortunately we have not been able to obtain experimental confirmation of these trends from the RET data for He and Ne collisions. In our experiments the odd ΔJ transitions for CO+He or Ne are masked by the even ΔJ propensity of the concurrent CO+CO collisions.

V. SUMMARY

Time-resolved pump–probe measurements were used to examine CO+Ne rotational energy transfer within the CO $\nu=2$ rotational manifold. Rotational levels in the range $J_i=2-9$ were excited and transfer of population to the levels $J_f=2-8$ was monitored. The resulting data set was analyzed by fitting to numerical solutions of the master equation. State-to-state rate constant matrices were generated using fitting law functions and *ab initio* theoretical calculations that employed a CCSD(T) potential energy surface.[15] The MEG fitting law and the theoretical rate constants yielded acceptable simulations of the kinetic data. However, only the latter were able to reproduce both the kinetic data and pressure broadening coefficients for CO+Ne. In this respect the conclusions of the present work are closely aligned to those derived from our recent work on CO+He. Again we find that correlations in fitting rate constant matrices to RET kinetics or pressure broadening data alone can be greatly reduced when a simultaneous fit to both data sets is required. For both CO+Ne and CO+He the best rate constant matrices were obtained from high-level theoretical calculations, rather than empirical fitting procedures. The present study shows that current *ab initio* computational methods are capable of predicting the thermally averaged dynamics of CO+Ne with near quantitative accuracy.

ACKNOWLEDGMENTS

[1] G. Winnewisser, B. S. Dumesh, I. Pak, L. Surin, F. Lewen, D. A. Roth, and F. S. Rusin, J. Mol. Spectrosc. **192**, 243 (1998).

[2] K. A. Walker, T. Ogata, W. Jäger, M. C. L. Gerry, and I. Ozier, J. Chem. Phys. **106**, 7519 (1997).

[3] R. W. Randall, A. J. Cliffe, B. J. Howard, and A. R. W. McKellar, Mol. Phys. **79**, 1113 (1993).

[4] A. R. W. McKellar and M. C. Chan, Mol. Phys. **93**, 253 (1998).

[5] R. B. Nerf, Jr. and M. A. Sonnenberg, J. Mol. Spectrosc. **58**, 474 (1975).

[6] A. Henry, D. Hurtmans, M. Margottin-Maclou, and A. J. Valentin, J. Quant. Spectrosc. Radiat. Transf. **56**, 647 (1996).

[7] R. Moszynski, T. Korona, T. G. A. Heijmen, P. E. S. Wormer, A. van der Avoird, and B. Schramm, Pol. J. Chem. **72**, 1479 (1998).

[8] K. Vatter, H. J. Schmidt, E. Elias, and B. Schramm, Ber. Bunsenges. Phys. Chem. **100**, 73 (1996).

[9] J. Kestin, S. T. Ros, and W. A. Wakeham, Ber. Bunsenges. Phys. Chem. **86**, 753 (1982).

[10] R. D. Trengrove, H. L. Robjohns, and P. J. Dunlop, Ber. Bunsenges. Phys. Chem. **88**, 450 (1984).

[11] N. Imaishi and J. Kestin, J. Phys. A **126**, 98 (1984).

[12] S. Antonova, A. Lin, A. P. Tsakotellis, and G. C. McBane, J. Chem. Phys. **110**, 11 742 (1999).

[13] K. T. Lorenz, D. W. Chandler, and G. C. McBane, J. Phys. Chem. A **106**, 1144 (2002).

[14] R. Moszynski, T. Korona, P. E. S. Wormer, and A. van der Avoird, J. Phys. Chem. A **101**, 4690 (1997).

[15] G. C. McBane and S. M. Cybulski, J. Chem. Phys. **110**, 11 734 (1999).

[16] V. Subramanian, K. Chitra, D. Sivanesan, R. Amutha, and S. Sankar, Chem. Phys. Lett. **307**, 493 (1999).

[17] S. P. Phipps, T. C. Smith, G. D. Hager, M. C. Heaven, J. K. McIver, and W. G. Rudolph, J. Chem. Phys. **116**, 9281 (2002).

[18] T. C. Smith, D. A. Hostutler, G. D. Hager, M. C. Heaven, and G. C. McBane, J. Chem. Phys. **120**, 2285 (2004).

[19] (a) J. J. Klaassen, S. L. Coy, J. I. Steinfeld, and B. Abel, J. Chem. Phys. **101**, 10 533 (1994); (b) J. J. Klaassen, S. L. Coy, J. I. Steinfeld, and Ch. Roche, *ibid.* **100**, 5519 (1994); (c) C. C. Flannery, J. I. Steinfeld, and R. R. Gamache, *ibid.* **99**, 6495 (1993).

[20] M. L. Koszykowski, L. A. Rahn, R. E. Palmer, and M. E. Coltrin, J. Phys. Chem. **91**, 41 (1987).

[21] J. P. Looney, G. J. Rosasco, L. A. Rahn, W. S. Hurst, and J. W. Hahn, Chem. Phys. Lett. **161**, 232 (1989).

[22] J. I. Steinfeld, P. Ruttenberg, G. Millot, G. Fanjoux, and B. Lavorel, J. Phys. Chem. **95**, 9638 (1991), and references therein.

[23] B. C. Sanctuary, Chem. Phys. Lett. **62**, 378 (1979).

[24] J. M. Hutson and S. Green, computer code MOLSCAT, version 14, distributed by Collaborative Computational Project No. 6 of the Engineering and Physical Sciences Research Council, UK, 1994.

[25] A. G. Maki, J. S. Wells, and D. A. Jennings, J. Mol. Spectrosc. **144**, 224 (1990).

[26] M. H. Alexander and D. E. Manolopoulos, J. Chem. Phys. **86**, 2044 (1987).

[27] P. McGuire and D. J. Kouri, J. Chem. Phys. **60**, 2488 (1974).

[28] J. J. BelBruno, J. Gelfand, and H. Rabitz, J. Chem. Phys. **78**, 3990 (1983).

[29] J. I. Steinfeld and R. R. Gamache, Spectrochim. Acta, Part A **54**, 65 (1998).

[30] S. Green, J. Chem. Phys. **70**, 4686 (1979).

[31] R. Shafer and R. G. Gordon, J. Chem. Phys. **58**, 5422 (1973).

[32] J.-P. Bouanich, J. Quant. Spectrosc. Radiat. Transf. **12**, 1609 (1972).

[33] T. G. A. Heijmen, R. Moszynski, P. E. S. Wormer, and A. van der Avoird, J. Chem. Phys. **107**, 9921 (1997).